Nuclear Engineering and Technology xxx (xxxx) xxx

Contents lists available at ScienceDirect

Nuclear Engineering and Technology

journal homepage: www.elsevier.com/locate/net

Design and analysis of isolation effectiveness for three-dimensional base-seismic isolation of nuclear island building

Xiuyun Zhu [a, b, *], Gao Lin [a], Rong Pan [b], Jianbo Li [a]

[a] Institute of Earthquake Engineering, Faculty of Infrastructure Engineering, Dalian University of Technology, Dalian, 116024, Liaoning, China
[b] Nuclear and Radiation Safety Center, Ministry of Ecology and Environment of PRC, Beijing, 100082, China

a r t i c l e i n f o

Article history:
Received 26 October 2020
Received in revised form
15 June 2021
Accepted 14 July 2021
Available online xxx

Keywords:
Base-seismic isolation
3-Dimensional combined isolation bearing (3D-CIB)
Nuclear island (NI) building
Seismic response
Isolation effectiveness

a b s t r a c t

In order to investigate the application of 3D base-seismic isolation system in nuclear power plants (NPPs), comprehensive analysis of constitution and design theory for 3-dimensional combined isolation bearing (3D-CIB) was presented and derived. Four different vertical stiffness of 3D-CIB was designed to isolate the nuclear island (NI) building. This paper aimed at investigating the isolation effectiveness of 3D-CIB through modal analysis and dynamic time-history analysis. Numerical results in terms of dynamic response of 3D-CIB, relative displacement response, acceleration and floor response spectra (FRS) of the superstructure were compared to validate the reliability of 3D-CIB in mitigating seismic response. The results showed that 3D-CIB can significantly attenuate the horizontal acceleration response, and a fair amount of the vertical acceleration response reduction of the upper structure was still observed. 3D-CIB plays a significant role in reducing the horizontal and vertical FRS, the vertical FRS basically do not vary with the floor height. The smaller the vertical stiffness of 3D-CIB is, the better the vertical isolation effectiveness is, whereas, it will increase the displacement and the rocking effect of superstructure. Although the advantage of 3D-CIB is that the vertical stiffness can be flexibly adjusted, it should be designed by properly accounting for the balance between the isolation effectiveness and displacement control including rocking effect. The results of this study can provide the technical basis and guidance for the application of 3D-CIB to engineering structure.

1. Introduction

The seismic base isolation system has been studied extensively in the last fifty years by a number of national and international academic and research institutions and has emerged as one of the most effective strategies to protect infrastructure from seismic hazards, especially in the high seismic region. So far, there are many types of base isolation systems successfully developed to reduce the disasters of earthquakes [1e5]. Although the isolation technology has been widely deployed for buildings, bridges and certain classes of infrastructure, it has yet to be routinely adopted for the seismic protection of nuclear power plants (NPPs). The reason for the limited use of seismic isolation to NPPs, development and future research needs was presented and identified [6,7]. The limited numbers of applications to NPPs to date have been in France and South Africa, for which neoprene rubber bearings, including flat sliders in some installations have been used to isolate the NPPs from the horizontal components of ground motion [8,9]. Conventional isolation systems are generally intended to reduce seismic horizontal demands, however, they do not prevent vertical seismic force from being transmitted directly into the superstructure and may even amplify the vertical seismic response [10]. Experimental studies conducted using shake table tests and field observation from seismic reconnaissance activities show that the vertical earthquake can cause serious structural and non-structural damage, especially for the high earthquake intensity zone whose vertical component of ground motion larger than the horizontal component [11e13]. Therefore, it is beneficial that a few isolation systems were invented to provide vertical isolation. Devices such as the rolling seal type air spring [14e16], hydraulic isolation systems [17], coned disk spring [18e20] were developed to provide the vertical isolation. In order to achieve the effectiveness of 3-dimensional (3D) seismic isolation, they are proposed to be

* Corresponding author. Institute of Earthquake Engineering, Faculty of infrastructure Engineering, Dalian University of Technology, Dalian, 116024, Liaoning, China.
E-mail addresses: lyzhuxiuyun@163.com (X. Zhu), gaolin@dlut.edu.cn (G. Lin), panrong@chinansc.cn (R. Pan), jianboli@dlut.edu.cn (J. Li).

https://doi.org/10.1016/j.net.2021.07.018

combined with the horizontal isolation component. Of course, other complete 3D seismic isolation systems such as the thick rubber layer bearings [21,22] and large helical springs [23] can provide flexibility in both the horizontal and vertical directions simultaneously. Besides, a new type of seismic isolation system known as periodic foundation adopts the concept of frequency band gap in periodic materials, which can isolate seismic waves in both horizontal and vertical directions [24,25].

Although 3D base-seismic isolation has not been applied to engineering practice of NPPs, for the sites which go beyond the input ground motion of the seismic standardization plant design, it can be accepted without changing the original standard design of structure and equipment by selecting the corresponding 3D isolation system to adjust its aseismic. Hence, 3D seismic isolation systems for safety-related nuclear structure [15,17,24e26] has become a great concern of research, which can provide the technical basis for code or standard and promote 3D base isolation to be practical application of NPPs for the regions with high seismic hazard.

For this purpose, a new 3D combined isolation bearing (3D-CIB) composed of laminated rubber bearing (LRB) and combined disk spring bearing (CDSB) is proposed and designed to isolate NI building in this paper. Different from the traditional disk spring bearing only including one disk spring column [18e20], CDSB is composed of one main column and several auxiliary columns of coned disk spring in parallel. The advantage of CDSB is the constitution can be flexibly adjusted according to the requirement of bearing capacity and vertical stiffness. Since CDSB can provide low vertical stiffness to decouple the superstructure from the vertical component of ground motion, it is selected as the vertical isolation device. This study begins with the comprehensive analysis of constitution and design theory for CDSB, and four different vertical stiffness of CDSB is designed to investigate the influence on the isolation effectiveness. Subsequently, modal analysis and nonlinear time-history analyses of 3D isolated NI building with different vertical stiffness are performed. Finally, the numerical results in terms of dynamic response of 3D-CIB, displacement response, acceleration and floor response spectra (FRS) of superstructure are compared to validate the reliability of 3D-CIB in mitigating seismic response.

2. Design of 3D combined isolation bearing (3D-CIB)

2.1. Design theory of CDSB

The main column of disk spring is located in the center, and the auxiliary columns are uniformly distributed on a large circle with a certain radius. The main column and auxiliary columns are all equipped with central guide tubes, and the bottom of each central guide tubes is rigidly connected to the bottom connection plate. The upper part of each main and auxiliary column is connected to a guide sleeve, which is integrated with the top connection plate. It is worth noting that the number of auxiliary columns can be flexibly adjusted according to the requirements of bearing capacity and vertical stiffness. Due to the large weight of the superstructure, i.e.NI building, eight auxiliary columns were selected for the constitution of CDSB in this paper, which the typical plan and section view of this CDSB is illustrated in Fig. 1.

Usually, single coned disk spring is divided into two types i.e. with and without bearing surface. For coned disk spring with relatively large thickness, the disk spring with bearing surface is generally selected. Compound combination of coned disk springs is adopted for CDSB. The coned disk springs of the same shape are stacked in parallel, and then this set is piled up. The main column is composed by stacking n_C coned disk springs in parallel and then i_C sets in series, which means the main column is made up $n_C \times i_C$ coned disk springs in total. Similarly, each auxiliary column was composed of the stack of n_S coned disk springs in parallel, and then i_S sets in series. The geometrical parameters of coned disk spring with bearing surface including outer diameter (D), inner diameter (d), thickness of the bearing surface (t') and inner coned height (h'), are shown in Fig. 2. Accordingly, the above parameters for the main and auxiliary coned disk spring are marked as $D_C d_C$, t'_C, h'_C and D_S, d_S, t'_S, h'_S, respectively.

The theory of disk spring was first presented by Almen and Laszlo [27] and then it was also recommended to the existing national standard of the coned disk spring [28]. Taking the main coned disk spring as an example, when the vertical load F_C acts on the inner circumference of coned disk spring, the deformation f_C occurs, the relationship between F_C and f_C is expressed as follows:

$$F_C = \frac{4E}{1-m^2}\$\frac{t_C'^4}{K_1 D_C^2}\$K_4^2\frac{f_C}{t'_C}\left[K_4^2\left(\frac{h'_C}{t'_C}-\frac{f_C}{t'_C}\right)\left(\frac{h'_C}{t'_C}-\frac{f_C}{2t'_C}\right)+1\right] \quad (1)$$

where, E is elasticity modulus, m is Poisson's ratio, K_1 andK_4 are calculation coefficients.

When the main disk spring is flattened, i.e.$f_C = h'_C$, Eq. (1) yields the critical load of single disk spring F_{Cc}, as follows

$$F_{Cc} = F_{(f_C = h'_C)} = \frac{4E}{1-m^2}\$\frac{t_C'^3 h'_C}{K_1 D_C^2}\$K_4^2 \quad (2)$$

The critical load of single auxiliary disk spring F_{Sc} can also be obtained in the same way. The critical load of each main and auxiliary column can be derived as $F_{VC} = n_C F_{Cc}$ and $F_{VS} = n_S F_{Sc}$,

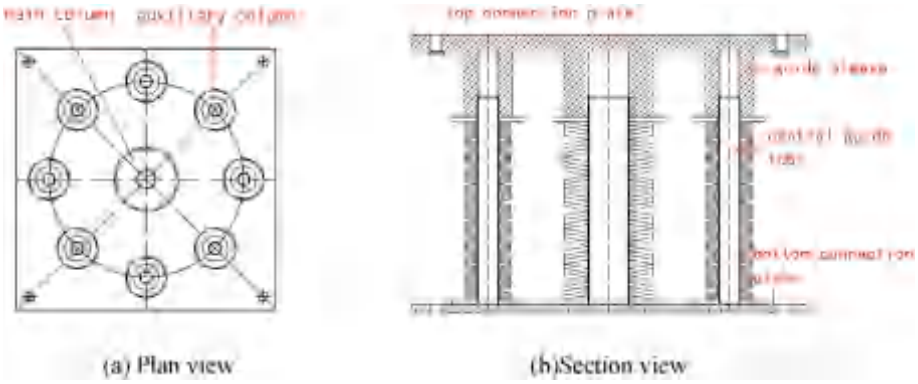

Fig. 1. Structural composition of combined disk spring bearing(CDSB).

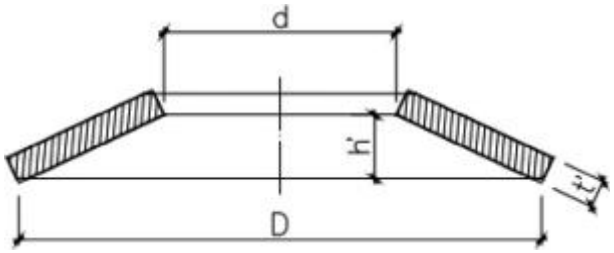

Fig. 2. Structure size of single disk spring with bearing surface.

respectively. Finally, the critical load of single CDSB can be expressed as follows.

$$F_{CDSBc} = F_{VC} + 8F_{VS} = n_C F_{Cc} + 8n_S F_{Sc} \tag{3}$$

It is assumed that the weight of the superstructure borne by single CDSB is defined as F. According to the scale factor of $m = F/F_{CDBSc}$ and $K_4(h'_C/t'_C)$, the ratio of the preloading initial deformation to the inner cone height f_C/h'_C can be obtained from characteristic curve of single disk spring. Then, the preloading initial deformation of CDSB can be obtained as $f_{CDSB} = i_C f_C = i_S f_S$.

According to the stiffness definition of single coned disk spring, under the initially deformation of the main disk spring f_C, its vertical stiffness K_C can be derived as follows:

$$K_C = \frac{dF_C}{df_C} = \frac{4E}{1-\mu^2}\frac{t'^3_C}{K_1 D_C^2}K_4^2\left\{K_4^2\left[\left(\frac{h'_C}{t'_C}\right)^2 - 3\left(\frac{h'_C}{t'_C}\right)\times\left(\frac{f_C}{t'_C}\right) + \frac{3}{2}\left(\frac{f_C}{t'_C}\right)^2\right] + 1\right\} \tag{4}$$

Further, the vertical stiffness of main and auxiliary column of disk spring can be inferred as follows:

$$\begin{aligned} K_{VC} &= n_C K_C / i_C \\ K_{VS} &= n_S K_S / i_S \end{aligned} \tag{5}$$

Finally, the total vertical stiffness of single CDSB is gotten as follows:

$$K_{V\,CDSB} = K_{VC} + 8K_{VS} \tag{6}$$

2.2. Design parameters of CDSB

Owing to the large weight of NI building whose total mass is 279,160 t, a total of 479 bearings were set. The average load borne by each bearing was 5718 kN. After the trial calculation, the geometrical parameters of coned disk spring with bearing surface were finally confirmed, as shown in Table 1. According to Eq. (1), the load and displacement relationship curves of the single main and auxiliary disk spring can be obtained, as shown in Fig. 3(a). It is exhibited that the two graphs are basically linear, and under the condition of $f_C = h'_C = 11{:}63$mm and $f_S = h'_S = 5{:}81$mm, the critical load of the single main and auxiliary disk spring is $F_{Cc} = 1245{:}0$ kN and $F_{Sc} = 311{:}25$ kN, respectively. Due to the requirement of bearing capacity, the parameter of n_C and n_S is set to be 3. Resultantly, the critical load of each main and auxiliary column is $F_{VC} = 3735{:}0$ kN and $F_{VS} = 933{:}75$ kN, respectively. According to Eq. (3), the critical load of each CDSB is $F_{CDSBc} = 11205{:}0$ kN.

According to the characteristic curve of the coned disk spring, the preloading initial displacement of the main and auxiliary disk spring was found to be 5.23 mm and 2.62 mm, respectively. According to Eq. (4), the vertical stiffness of single main and auxiliary coned disk spring is $K_C = 1{:}056 \times 10^8$N/m and $K_S = 1/2K_C$, respectively. It can be seen from Eq. (5) and Eq. (6) that the vertical stiffness of CDSB can be flexibly adjusted according to the number of sets in series, on the premise that $n_C = n_S = 3$ and $m = 8$ have been determined. To investigate the influence of different vertical stiffness of CDSB on the seismic response and isolation effectiveness, four different sets in series were designed, i.e. $i_C = 4; 6; 10; 16$ and $i_S = 2i_C = 8; 12; 20; 32$, and recorded as CDSB1, CDSB2, CDSB3, CDSB4, respectively. Further, the combination process of stiffness from single disk spring to CDSB is shown in Table 2. Moreover, the load and displacement relationship curves of the main column of CDSB are plotted in Fig. 3(b). It is observed that when the main column of CDSB is flattened, i.e. the vertical displacement of CDSB1, CDSB2, CDSB3 and CDSB4 reaches 46.5, 69.8, 116.3 and 186.0 mm, the critical load of the corresponding main column is the same, i.e. $F_{VC} = 3735{:}0$ kN. According to Eq. (3), the load and displacement relationship curves of CDSB are shown in Fig. 3(c), the critical load of CDSB is also the same, i.e. $F_{CDSB1} = F_{CDSB2} = F_{CDSB3} = F_{CDSB4} = 11205{:}0$ kN.

Note that in this study, equivalent damping ratio of CDSB was assumed to be 0.2. This value was selected because the test results

Table 1
Characteristic parameter of single disk spring unit: mm.

Type	D	d	t′	h′
Main disk spring	400	133.3	23.25	11.63
Auxiliary disk spring	200	66.7	11.63	5.81

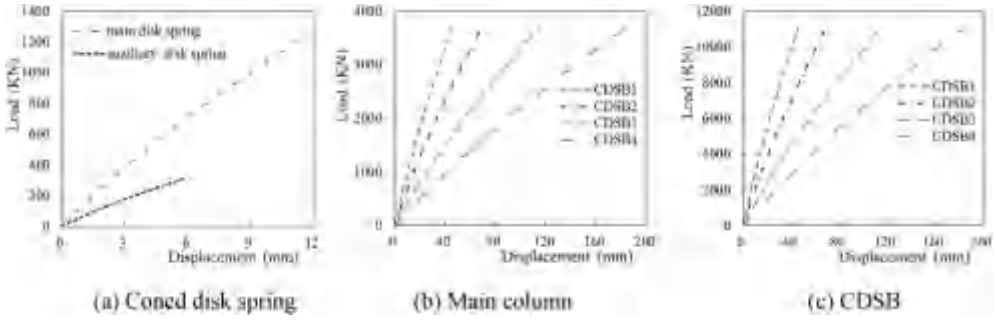

Fig. 3. Load-displacement curves.

Table 2
The combination process of stiffness from single disk spring to CDSB.

Type	$n_C = n_S$	i_C=i_S	K_C (N/m)	K_{VC} (N/m)	$K_{V\,CDSB}$ (N/m)	$K_{V\,LRB-CDSB}$ (N/m)
CDSB1	3	4/8	1.056×10^8	7.922×10^7	2.377×10^8	2.233×10^8
CDSB2	3	6/12	1.056×10^8	5.281×10^7	1.584×10^8	1.519×10^8
CDSB3	3	10/20	1.056×10^8	3.167×10^7	9.506×10^7	9.269×10^7
CDSB4	3	16/32	1.056×10^8	1.980×10^7	5.941×10^7	5.848×10^7

showed that CDSB itself has a certain high damping ratio, i.e. 0.2e0.3 due to large number of coned disk springs stacked [29]. Of course, the equivalent damping ratio of CDSB is an important parameter. It is necessary to conduct a performance test to measure the equivalent damping ratio for the practical application of CDSB.

2.3. Design theory of 3D-CIB

3D-CIB is composed of two parts, which the LRB and CDSB are used as the horizontal and vertical isolation component, respectively. They are piled up in series by high-strength bolts, as shown Fig. 4. As a combination in series, this 3D-CIB is also figuratively marked as LRB-CDSB. The LRB has small horizontal stiffness and high vertical stiffness, whereas the CDSB performs high horizontal stiffness and its vertical stiffness is much lower than that of LRB. In this way, it can be inferred that the horizontal stiffness ($K_{H\,LRB-CDSB}$) only considers the horizontal stiffness of LRB ($K_{H\,LRB}$), and the vertical stiffness ($K_{V\,LRB-CDSB}$) is calculated according to a series combination of LRB and CDSB. Hence, the horizontal and vertical stiffness of LRB-CDSB can be obtained as follows.

$$\begin{aligned} K_{H\,LRB-CDSB} &= K_{H\,LRB} \\ K_{V\,LRB-CDSB} &= K_{V\,LRB}K_{V\,CDSB}/(K_{V\,LRB} + K_{V\,CDSB}) \end{aligned} \tag{7}$$

In this study, LRB with an additional lead core was adopted, with the vertical stiffness $K_{V\,LRB} = 3{:}712 \times 10^9$N/m, initial stiffness before yield $K_u = 1{:}5 \times 10^7$N/m, the stiffness after yield $K_d = 1{:}4 \times 10^6$N/m, equivalent stiffness $K_{eq} = 2{:}35 \times 10^6$N/m, yield load $Q_d =$ 140 kN, equivalent damping ratio $\zeta_{eq} = 0{:}25$, and ultimate shear deformation $D_{ult} =$ 40cm. LRB individually combined with CDSB1, CDSB2, CDSB3 and CDSB4 in series is marked as LRB-CDSB1, LRB-CDSB2, LRB-CDSB3 and LRB-CDSB4, respectively. According to Eq. (7), the vertical stiffness of LRB-CDSB is listed in the last column of Table 2.

3. Basic data for seismic analysis

3.1. Model of 3D isolated NI building

In this study, NI building of reinforced frame and shear wall structure with eight floors was selected as the superstructure. The elevations for each floor are EL. 3.0, 9.25, 15.75, 23.25, 29.05, 34.45, 42.65, 49.15 and 60.65 m, respectively. The thicknesses of floor at EL.9.25 m and other elevations is 0.6 m and 0.5 m, respectively. The thicknesses of exterior walls from the bottom to the top vary among 1.7, 1.6, 1.5, 1.2, 1.0, 0.7, 0.4 and 0.3 m. The commercial finite element (FE) software of ANSYS was employed to establish the model of NI building, as shown in Fig. 5. The element type of Solid 185 suit for modeling solid structure was used to model the raft foundation with thickness of 5.5 m (EL. −2.5e3.0 m). The floors, roof and walls were modeled by element type of Shell 181, which is suit for analyzing thin to moderately thick shell structure. The element type of Beam188 based on Timoshenko theory including shear-deformation effects was used to simulate beam, column and steel truss of roof. The element type of Mass21 was used to simulate the lumped nonstructural mass attached to the floor. It is noted that the internal structure inside the containment was simulated by lumped mass stick model, the mass and moment of inertia of which are all concentrated at floor elevation and modeled using Mass21. The inertial moment and shear area between two adjacent floors are represented by beam elements Beam188. It is an established fact that the response of the structure is sensitive to mesh size for the FE method. Accordingly, refer to FE model of AP1000 NI building for dynamic analysis, which the mesh size of shell element for wall and floor was about 10 feet [30], the size of shell and solid element in this FE model was meshed as approximately 2e3.5 m.

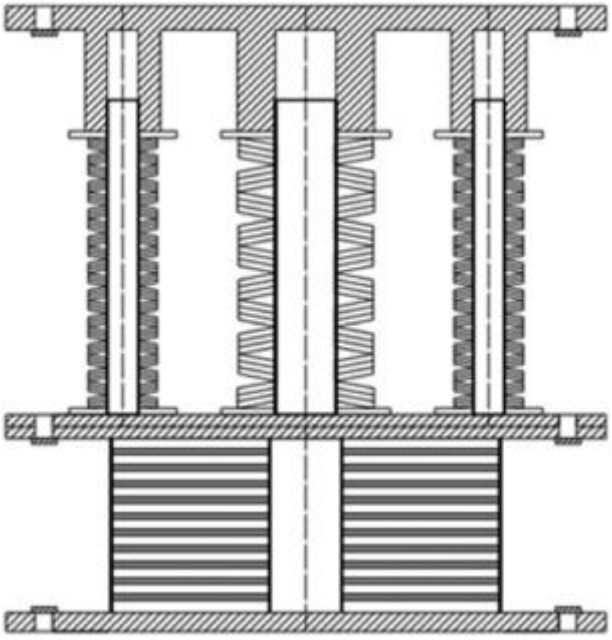

Fig. 4. Section view of 3D combined isolation bearing(3D-CIB).

A total of 479 isolation bearings were set beneath the raft foundation whose length and width was 54.9 and 57.9 m, respectively. The plane layout of 3D-CIB is shown in Fig. 6. The horizontal and vertical behavior of 3D-CIB was simulated by nonlinear and linear spring-damper element, respectively. The element type of COMBIN40, in which two spring constants (K1 and K2), damping coefficient (C), mass constant (M), gap size (GAP) and limiting sliding force (FSLIDE) was adopted to simulate the horizontal behavior. The relationship among initial stiffness K_u, K1 and K2 is that $K_u = K1 + K2$. For COMBIN40, both the bilinear strengthening model and the effect of viscous damping are considered, and mass constant (M) and gap size (GAP) are set to zero for isolators. The element type of COMBIN14 whose real constants include spring constant (K) and damping coefficient (C_V), is adopted to simulate the vertical characteristics. The geometry and mechanical model of COMBIN14 and COMBIN40 is shown in Fig. 7. Thus, the combination of one element of COMBIN14 and two elements of COMBIN40 was used to simulate 3D-CIB.

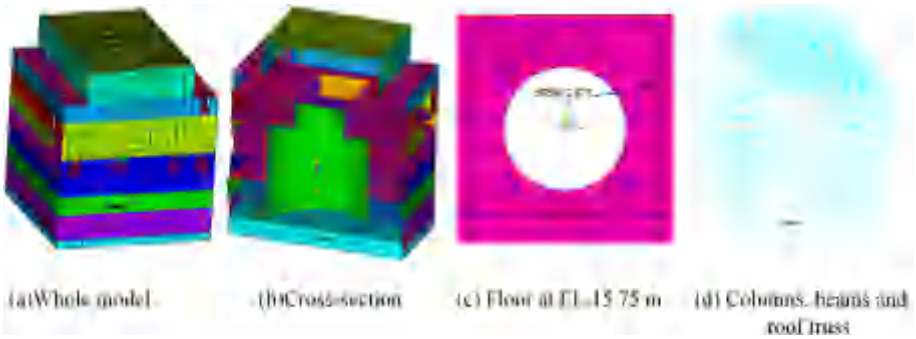

Fig. 5. Finite element model of NI building.

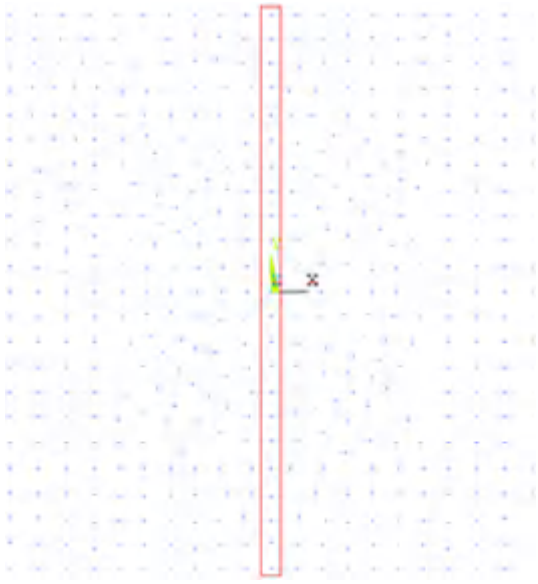

Fig. 6. Layout of discrete isolators under raft foundation.

3.2. Input ground motion

In this study, the three components of artificial acceleration time-history plotted in Fig. 8 are the input ground motion, whose corresponding response spectra for a damping ratio of 5% as shown in Fig. 9 are the design response spectra of Regulatory Guide 1.60 [31]. The peak ground acceleration in both horizontal and vertical directions is 2.943 m/s^2, i.e. 0.3 g (g = 9.81 m/s^2), the total duration and the time step is 28 s and 0.01 s, respectively. Each of the three components is statistically independent from the others. Based on that, the three components of ground motion were input simultaneously. According to Regulatory Guide 1.92 [32], the algebraic summation of seismic response for three directions is realized automatically.

4. Modal analysis

As the first step, modal analysis for non-isolated and 3D isolated NI building with the abovementioned different vertical stiffness was carried out. Consequently, the main frequencies and vibration modes reflecting the dynamic characteristics of the above models were obtained. The main frequencies are summarized in Table 3. In this table, "$U_X U_Y, U_Z$" denotes the degree of freedoms (DoFs) of translation in the X, Y, Z direction, respectively. "ROT_Z" denotes the DoF of torsion around the Z-axis. "Fixed" and "LRB-CDSB1" denote the results calculated by non-isolated and 3D isolated NI building with LRB-CDSB1, respectively.

As can be seen in Table 3, the natural frequencies of 3D isolated NI building for both the horizontal translation and torsional DoFs are significantly reduced compared to that of the non-isolated NI building. The horizontal isolation frequencies decreased slightly with a decrease in the vertical stiffness of LRB-CDSB. Therefore, it can be confirmed that the horizontal dynamic characteristics of 3D isolated structure are not only determined by horizontal stiffness of LRB-CDSB, but also are influenced by its vertical stiffness. Furthermore, the vertical frequency of 3D isolated NI building was also significantly reduced and decreased with a decrease in the vertical stiffness of LRB-CDSB. Due to the requirement of controlling the displacement response, the vertical isolation frequency is controlled for the range of 1.6e3.2 Hz in this paper.

5. Analysis of seismic isolation effectiveness

To comprehensively investigate the horizontal and vertical isolation effectiveness of 3D-CIB with different vertical stiffness, the nonlinear dynamic analysis of 3D base-seismic isolated NI building with different vertical stiffness were carried out. Accordingly, comparison analysis of seismic response in terms of dynamic response of 3D-CIB, displacement response, acceleration and FRS of the superstructure were conducted.

5.1. Dynamic response of 3D-CIB

A total of 479 isolation bearings were arranged beneath the raft foundation, the dynamic response of the center isolator is mainly discussed in this section. The horizontal and vertical displacement time histories of the center 3D-CIB with different vertical stiffness are illustrated in Fig. 10, and Table 4 shows the above peak displacements. It can be seen that the horizontal displacement responses of 3D-CIB with different vertical stiffness were almost the same with little difference, while the vertical displacement responses were quite different, they increased with a decrease in the vertical stiffness. Specially, the peak vertical displacement along the positive and negative direction of LRB-CDSB4 is 2.8 and 1.8 times that of LRB-CDSB1, respectively. For the coned disk spring, its vertical compression displacement is the focus of attention. As summarized in Table 4, it is found that the vertical compression displacement of LRB-CDSB1, LRB-CDSB2, LRB-CDSB3 and LRB-CDSB4 is 1.28, 1.64, 2.05 and 2.32 cm, converted into the displacement of single main disk spring is 3.19, 2.73, 2.05 and 1.45 mm, corresponding to 0:27h'_C, 0:23h'_C, 0:18h'_C and 0:12h'_C, respectively. Of course, the peak horizontal displacements of 3D-CIB are all less than 8 cm, which is far less than the ultimate shear deformation of

Fig. 7. The geometry and mechanical model of spring-damper element.

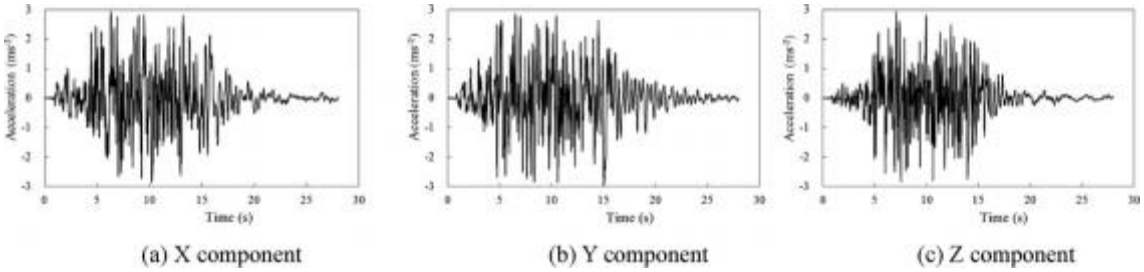

Fig. 8. The acceleration time histories of ground motion.

LRB, i.e., 40 cm.

A total of 23 bearings were arranged along Y-axis as shown Fig. 6, the peak values of vertical displacement are extracted and compared as shown in Fig. 11. The legends "LRB-CDSB1+" and "LRB-CDSB1 -" denote the relative displacement response in the positive and negative directions of coordinate axis, which is calculated by LRB-CDSB1. It is observed that the order of the peak displacement whether along the positive and negative direction of Z-axis is as follows, LRB-CDSB4 > LRB-CDSB3 > LRB-CDSB2 > LRB-CDSB1. It means the smaller the vertical stiffness is, the larger the vertical displacement amplitude of LRB-CDSB is. Moreover, compared with the center 3D-CIB, a little larger amplitude was observed for 3D-CIB located at outer edge. This increase of vertical displacement amplitude is caused by the rocking effect. In other words, the rocking effect can increase the vertical displacement demands for the 3D-CIB located closest to the outer edge.

On the other hand, the shear and axial force time histories of the center 3D-CIB with different vertical stiffness were illustrated in Fig. 12, and Table 4 listed the above peak forces. It can be seen that the shear force showed the limited difference, while an obvious difference for the axial force of 3D-CIB with different vertical stiffness was illustrated. Further, the axial force of 3D-CIB decreased with a decrease in the vertical stiffness, and the axial force of LRB-CDSB4 along the positive and negative direction was reduced by 51.3% and 26.4%, compared with that of LRB-CDSB1.

5.2. Displacement response of superstructure

The displacement responses of 3D isolated and non-isolated NI building relative to the ground are presented and discussed herein. The peak displacements of nodes with the same location as NODE 5954 and NODE 2473 at different floors were extracted and plotted in Fig. 13. As shown Fig.13 (a) and (b), the peak horizontal displacement of the non-isolated NI building was very small, and the maximum horizontal displacement of roof was only 2.7 cm. On the contrary, the peak horizontal displacement of 3D isolated NI building relative to the ground was significantly enlarged, and slightly amplified with the floor height due to little rocking. In particular, the amplification effect was more obvious with a decrease in the vertical stiffness. Hence, it can be inferred that the decrease in the vertical stiffness of LRB-CDSB may increase the rocking effect of superstructure, and then affect its horizontal displacement. The order of peak horizontal relative displacement and rocking effect is as follows: LRB-CDSB4 > LRB-CDSB3 > LRB-CDSB2 > LRB-CDSB1. For instance, 3D isolated NI building with LRB-CDSB4 performed the most serious rocking effect, the peak horizontal displacement of the roof relative to the raft foundation in the positive and negative direction of X axis, as shown in Fig. 13(a) was only 3.48 cm and 3.67 cm, respectively. Consequently, the corresponding rocking ratio was very small, less than 1/1250, which indicated that the rocking effect was not obvious.

In the vertical direction, it was observed from Fig. 13(c) that the displacement of the non-isolated NI building was very small, while the displacement of 3D isolated NI building was obviously amplified, and the peak values barely varied with the floor height. These characteristics demonstrated the uniform resistance to avoid vertical deformation similar to rigid body behavior. Furthermore, the vertical displacement responses increased with a decrease in the vertical stiffness of 3D-CIB.

5.3. Comparison of acceleration response

The acceleration responses of nodes with the same location as NODE 5954 and NODE 2473 at different floors were extracted, and the absolute peak values are plotted in Fig. 14. In general, it appeared that both the horizontal and vertical acceleration responses from the bottom to the top of 3D isolated NI building were basically not amplified, and the superstructure behaved overall vibration characteristics like a rigid body. In contrast, they increased rapidly with floor height of the non-isolated structure, especially for the horizontal direction.

Furthermore, a substantial reduction of horizontal peak acceleration responses is noted in comparison to the non-isolated structure. Especially for the roof of NI building, a response reduction of roughly 80% was found, which means the isolation effectiveness for the horizontal acceleration response is remarkable.

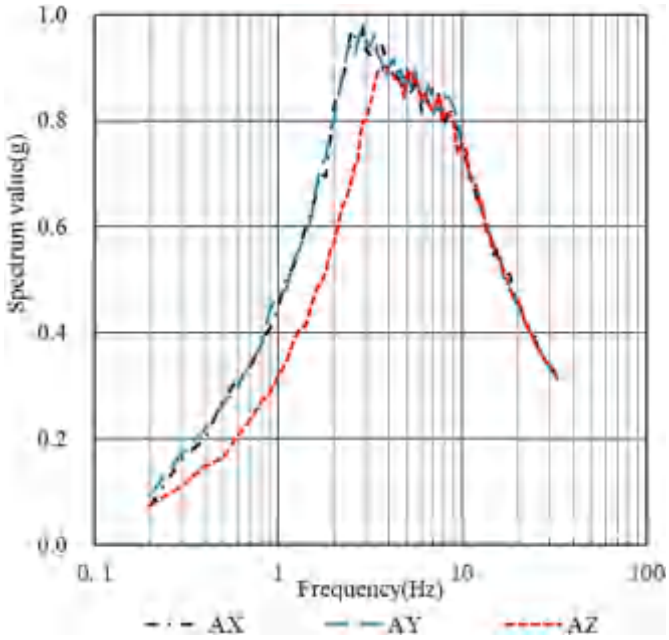

Fig. 9. The acceleration response spectra of ground motion.

Table 3
Comparison of the natural frequency of vibration unit: Hz

RANGE	MODE	LRB-CDSB1	LRB-CDSB2	LRB-CDSB3	LRB-CDSB4	Fixed
1	U_X	0.734	0.708	0.659	0.597	3.392
2	U_Y	0.740	0.717	0.673	0.615	3.527
3	ROT_Z	0.938	0.938	0.937	0.937	6.528
4	U_Z	3.148	2.545	2.098	1.587	7.302

Moreover, it was observed that the horizontal peak acceleration calculated by LRB-CDSB with different vertical stiffness was almost the same, which indicated that the horizontal acceleration response was predominantly influenced by the horizontal stiffness of 3D-CIB, and slightly influenced by the vertical stiffness.

As shown in Fig. 14(c), although the vertical response reduction of 3D isolated NI building was not as significant as that for the horizontal direction, a fair amount of response reduction of the upper structure was still observed. Additionally, it is clear that the vertical acceleration response decreased with a decrease in the vertical stiffness of 3D-CIB. Taking the nodes of sub top floor and top floor as examples, the substantial response reduction calculated by LRB-CDSB1, LRB-CDSB2, LRB-CDSB3 and LRB-CDSB4 is 42.4, 52.2, 64.4, and 64.8%, and 27.9, 33.6, 51.8, and 47.7%, respectively. On the other hand, the vertical acceleration time histories of NODE 2473 are depicted in Fig. 15. It is observed that the acceleration time history of non-isolated structure is the largest, whose peak value is 7.37 m/s^2, while the peak acceleration calculated by LRB-CDSB1, LRB-CDSB2, LRB-CDSB3 and LRB-CDSB4 is 5.53, 5.05, 3.56 and 3.73 m/s^2, respectively. Further, the shapes of acceleration time histories calculated by different LRB-CDSB are similar, but quite different from that of the non-isolated structure.

5.4. Floor response spectra (FRS) of superstructure

FRS including horizontal and vertical components is used as the input data of seismic design for the safety-related secondary mechanical, electrical, and piping systems. Comparison analysis of FRS is focused the support locations for safety-related secondary

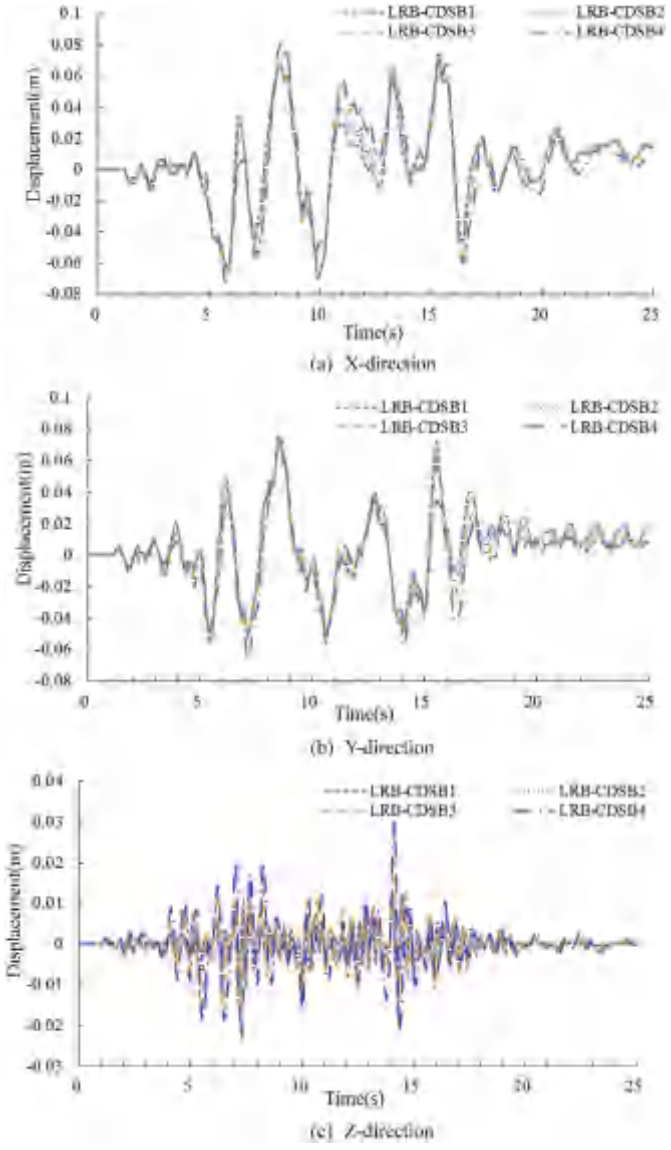

Fig. 10. Comparison of displacement time histories of the center 3D-CIB.

systems, so the node number of 5954 and 2473 located near the middle at the 3rd and the 6th floor with large span (EL. 15.75 and 34.45 m) as shown in Fig. 5(c), was selected herein. For brevity, the horizontal and vertical FRS of 5% critical damping ratio for NODE 5954 and NODE 2473 is compared as plotted in Fig. 16 and Fig. 17, respectively. Moreover, comparison of the spectral acceleration peak value (S_{max}), frequency (f) corresponding to S_{max}, reduction rate of S_{max} (d) and zero period acceleration (ZPA) of the vertical FRS is summarized in Table 5.

5.4.1. Analysis of FRS in horizontal direction

From the comparison of graphs in Fig. 16, it was observed that the first peak state of FRS calculated by 3D isolated structure occurs near the horizontal isolation frequency, and FRS at other frequencies greater than about 1.0 Hz is greatly reduced in comparison to that of the non-isolated structure. Moreover, the vertical stiffness of LRB-CDSB had a little influence on the horizontal FRS, especially for the NODE 5954 located at the lower floor, the spectral values were basically equivalent for the frequencies greater than 3.0 Hz. For NODE 2473, the spectral values at 1e10 Hz are slightly reduced

Table 4
Comparison of peak displacement and force of the center 3D-CIB.

TYPE	Displacement (cm)						Force (10^6N)					
	UX+	UX-	UY+	UY-	UZ+	UZ-	FX+	FX-	FY+	FY-	FZ+	FZ-
LRB-CDSB1	7.43	−7.03	7.57	−5.65	1.07	−1.28	0.562	−0.586	0.542	−0.642	3.008	−2.538
LRB-CDSB2	7.49	−6.69	7.50	−5.42	1.32	−1.64	0.513	−0.566	0.523	−0.607	2.682	−2.092
LRB-CDSB3	6.88	−6.73	7.14	−5.24	1.99	−2.05	0.511	−0.538	0.502	−0.590	2.055	−1.924
LRB-CDSB4	7.97	−7.17	6.94	−6.76	3.00	−2.32	0.525	−0.530	0.495	−0.534	1.465	−1.868

NOTE:"UX+" and "UX-" denote the peak displacement along the positive and negative direction of X-axis, respectively. "FX+" and "FX-" denote the peak force along the positive and negative direction of X-axis, respectively.

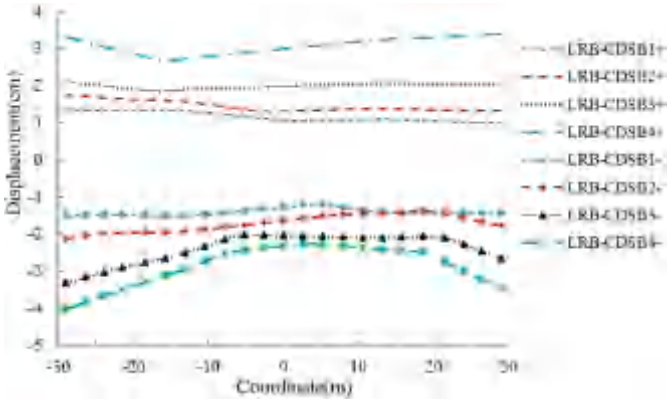

Fig. 11. Comparison of the vertical peak displacement response of 3D-CIB along Y axis.

with a decrease in the vertical stiffness of LRB-CDSB. Overall, the spectral peak values of 3D isolated structure are reduced by at least 80%, compared with that of non-isolated structure. In a word, it is confirmed that 3D base-seismic isolation of LRB-CDSB plays a significant role in reducing FRS in the horizontal direction.

5.4.2. Analysis of FRS in vertical direction

As can be seen from Fig. 17 and Table 5, the spectral peak values for 3D isolated structure with different vertical stiffness all obviously moved to lower frequencies (1.6e3.15 Hz), and the spectral values near the peak frequency and to the left of spectral peak are much larger than that of the non-isolated structure. In contrast, the spectral values of the high frequency range greater than approximately 4.0 Hz were obviously reduced. It is worth noting that the vertical dominant frequencies of most secondary systems are greater than the horizontal dominant frequency, and are far greater than the peak frequencies of vertical FRS, i.e. 1.6e3.15 Hz. Hence, it can be concluded that the peak values of FRS calculated by 3D isolated NI building can stagger the vertical dominant frequencies of most secondary systems. Consequently, although the spectral values of less than about 4.0 Hz are amplified, it barely produces adverse effect on the vertical seismic design of secondary systems.

Furthermore, it is clear that the spectral peak values become smaller and shift to lower frequencies, and the spectral values to the right of spectral peak also decreased with a decrease in the vertical stiffness. Specially, the order of the peak value and spectral values to the right of spectral peak is as follows LRB-CDSB1 > LRB-CDSB2 > LRB-CDSB3 > LRB-CDSB4. As summarized in Table 5, compared with the non-isolated NI building, the reduction ratio of spectral peak (ḍ) of NODE 2473 calculated by LRB-CDSB1, LRB-CDSB2, LRB-CDSB3 and LRB-CDSB4 is 29.7, 45.5, 59.8 and 67.8%, respectively. For NODE 5954, the spectral peak calculated by LRB-CDSB1 is increased by 12.7%, while the spectral peaks calculated by LRB-CDSB2, LRB-CDSB3 and LRB-CDSB4 are reduced by 9.1%, 32.5% and 44.9%, respectively. Thus, it is found that the vertical

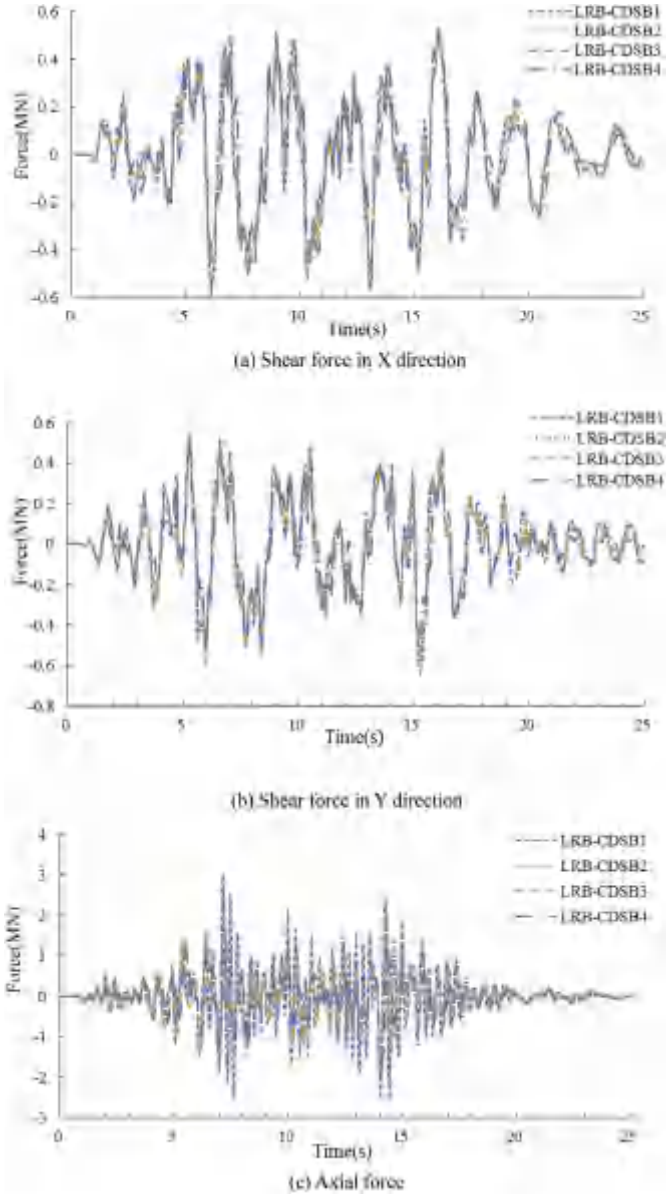

Fig. 12. Comparison of force time histories of the center 3D-CIB.

isolation effectiveness of higher floor is better than that of lower floor. Here, it should be noted that even though the spectral peak value calculated by LRB-CDSB1 is higher than that of non-isolated structure, it will only affect a small range of secondary systems with low frequency in vertical direction.

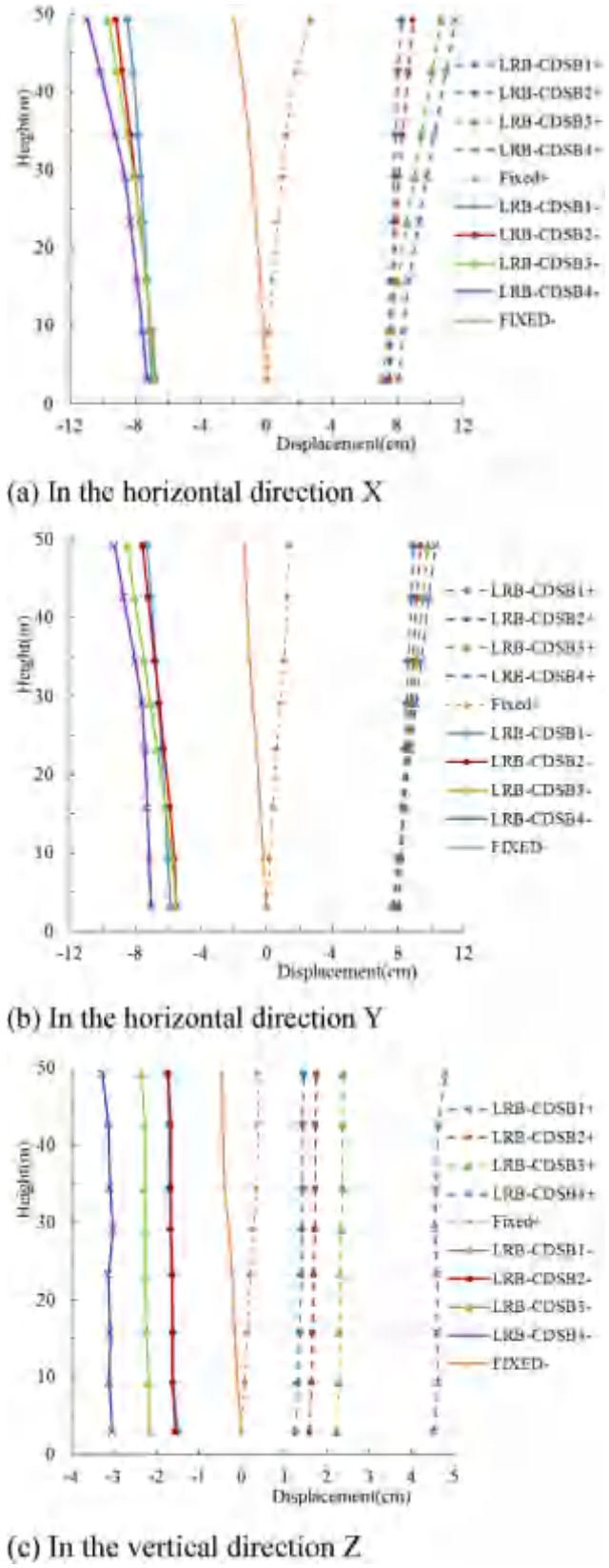

Fig. 13. Comparison of peak displacement response.

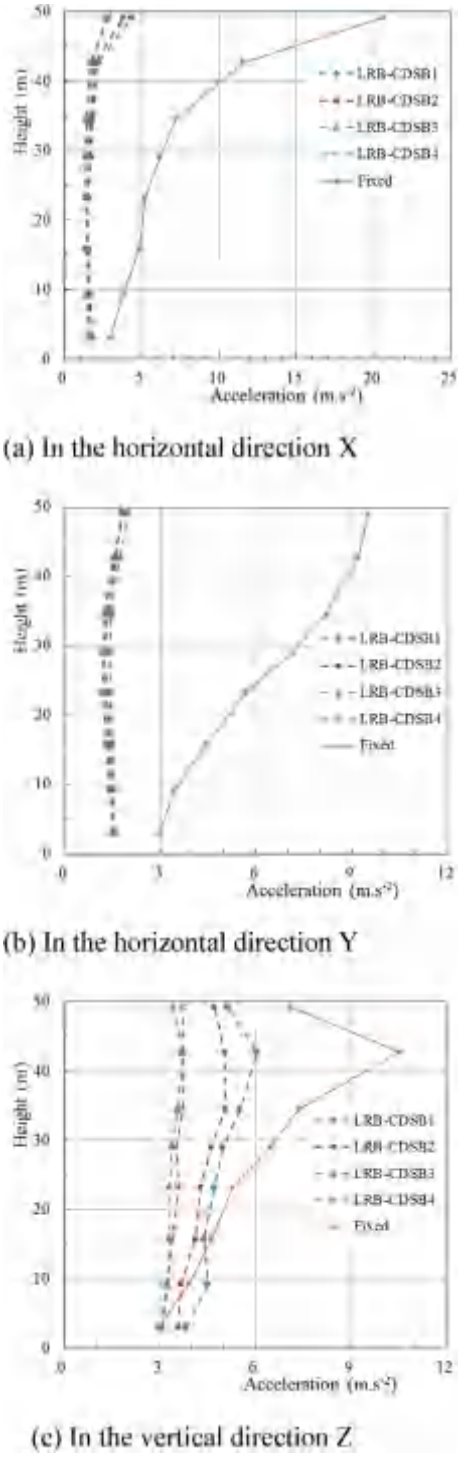

Fig. 14. Comparison of peak acceleration response.

5.4.3. Analysis of vertical FRS for different *f*loor height

To investigate the influence of different floor height on the vertical FRS, FRS of nodes with the same location as NODE 5954 and NODE 2473 at different floors were separately calculated for the non-isolated and 3D isolated NI building with LRB-CDSB3, and shown in Fig. 18. The spectral peak values (S_{max}), frequency (f) corresponding to S_{max}, and ZPA are listed in Table 6. For the non-isolated NI building, it exhibited that the peak values of FRS for different floors all occurred at 9.5 Hz, and the spectral value of greater than approximately 3.0 Hz increased with the increase of floor height. In particular, the spectral peak value and ZPA of node at EL. 42.65 m were enlarged by 2.88 times and 1.72 times,

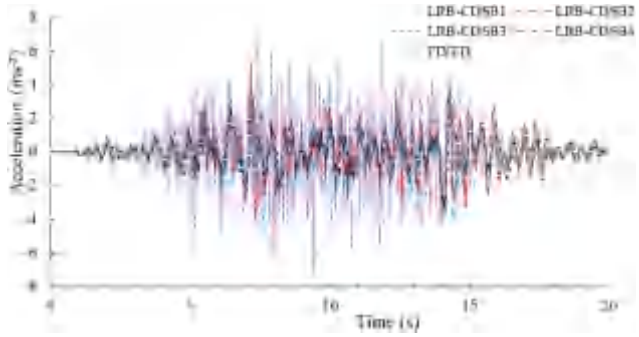

Fig. 15. Comparison of vertical acceleration time histories of NODE 2473.

compared with that of node at EL. 9.25 m, respectively. On the contrary, the spectral peak value for 3D isolated NI building all occurred at 2.2 Hz, and the peak values and ZPA basically did not vary with the floor height. The spectral peak values and ZPA of node at EL. 42.65 m were only amplified by 5% and 16%, compared with that of node at EL. 9.25 m. Furthermore, the spectral values of different height floor in the high frequency range of 8e20 Hz are a little different, and that of node at EL. 42.65 m is the largest. In summary, the above results indicated that under 3D base-seismic isolation, the spectral peak value and ZPA for nodes at different height floor are basically unchanged with the floor height, which is very beneficial to the vertical seismic design of secondary systems located on high floor.

6. Conclusions

Based on the advantage that constitution of CDSB can be flexibly adjusted according to the requirements of bearing capacity and vertical stiffness, four combinations of CDSB were designed to constitute 3D-CIB in this paper. Comparison analysis of vibration characteristics and dynamic responses between the non-isolated

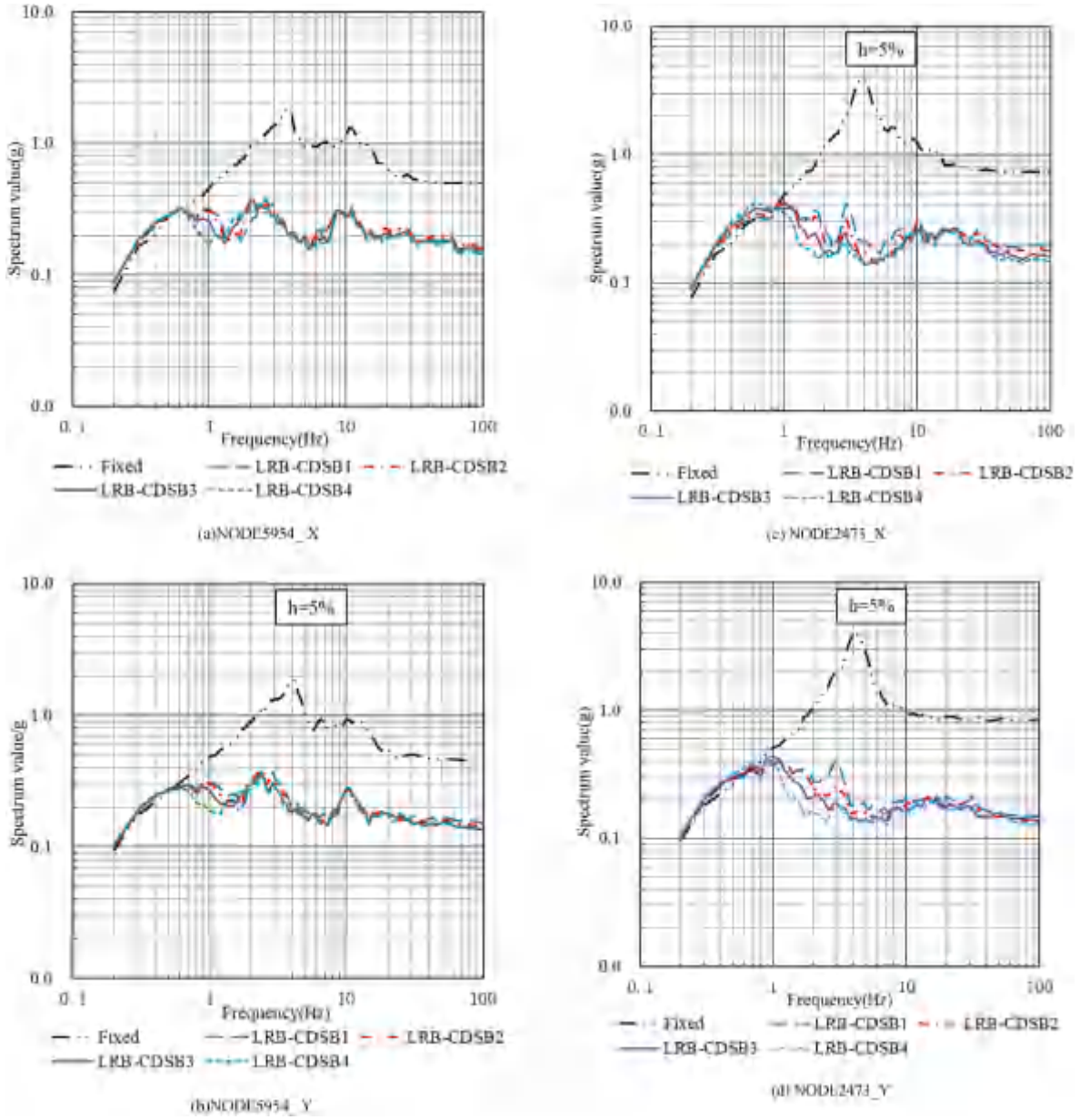

Fig. 16. Comparison of FRS in the horizontal direction.

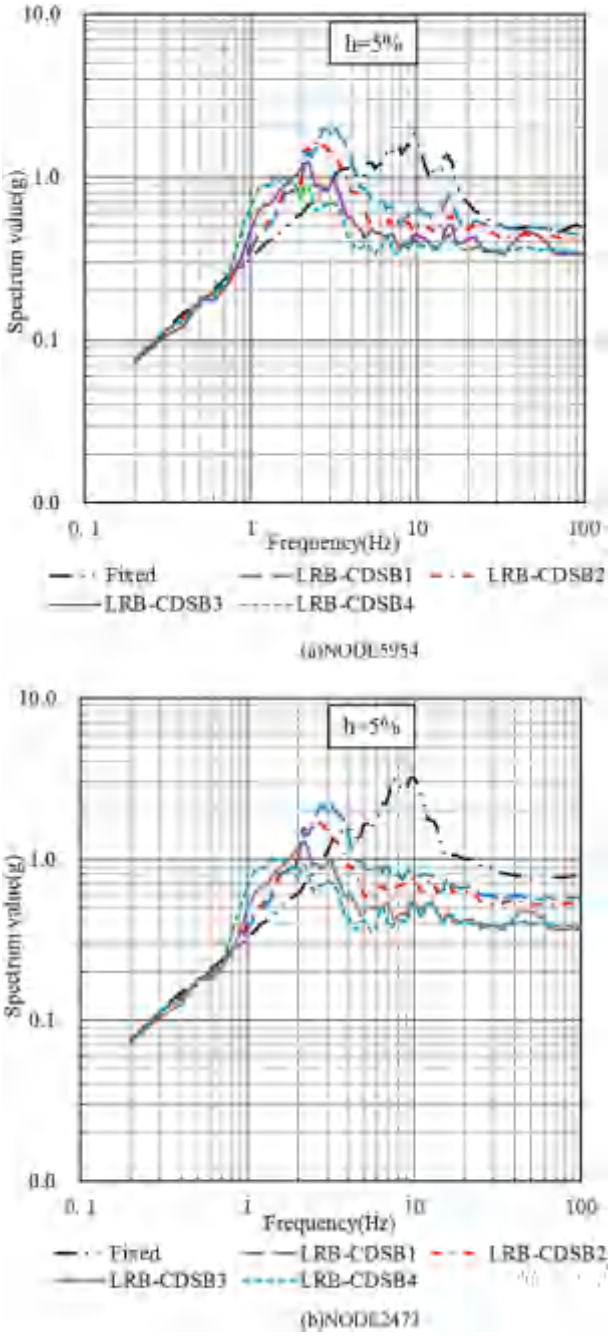

Fig. 17. Comparison of FRS in the vertical direction.

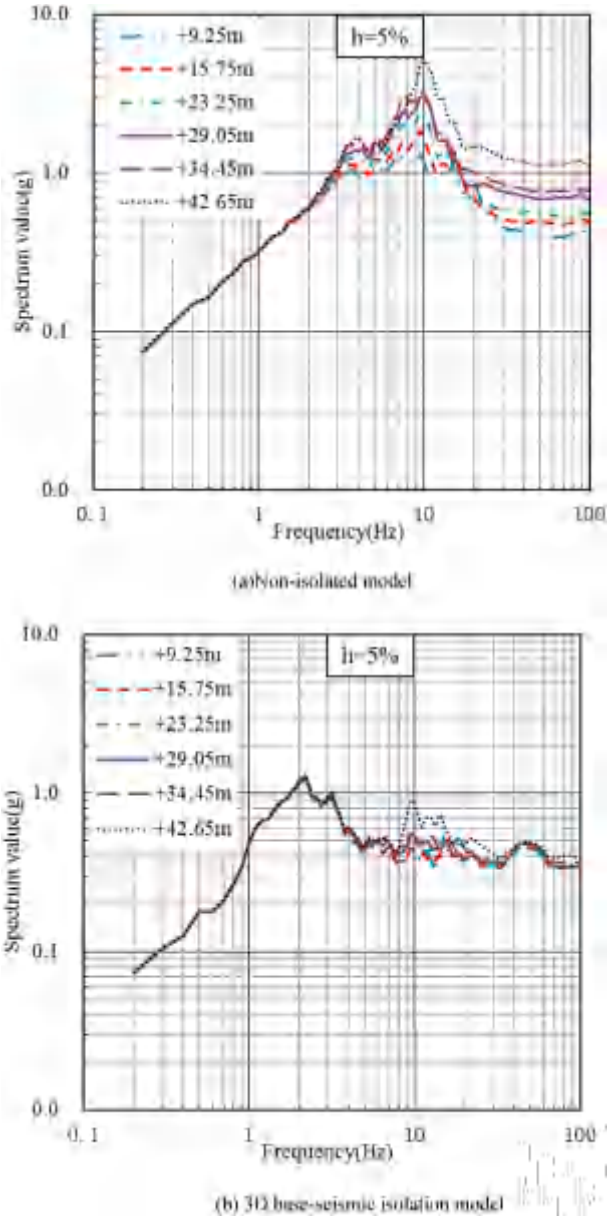

Fig. 18. Comparison of vertical FRS for floor nodes of different elevations.

Table 5
Comparison of peak value and corresponding frequency and ZPA of vertical FRS.

TYPE	NODE_5954			NODE_2473		
	S_{max}=f (g/Hz)	d	ZPA(g)	S_{max}=f (g/Hz)	d	ZPA(g)
LRB-CDSB1	2.093/3.15	+12.7%	0.450	2.274/3.15	−29.7%	0.568
LRB-CDSB2	1.688/2.5	−9.1%	0.424	1.763/2.5	−45.5%	0.522
LRB-CDSB3	1.253/2.2	−32.5%	0.339	1.301/2.2	−59.8%	0.364
LRB-CDSB4	1.024/1.6	−44.9%	0.346	1.041/1.6	−67.8%	0.381
Fixed	1.857/9.5	/	0.485	3.233/9.5	/	0.768

Table 6
Comparison of peak value and corresponding frequency and ZPA of vertical FRS for different elevations.

Elevation	S_{max}=f (g/Hz)		ZPA (g)	
	Fixed	LRB-CDSB3	Fixed	LRB-CDSB3
+9.25 m	1.317/9.5	1.229/2.2	0.407	0.334
+15.75 m	1.857/9.5	1.253/2.2	0.485	0.339
+23.25 m	2.477/9.5	1.271/2.2	0.550	0.338
+29.05 m	3.034/9.5	1.285/2.2	0.683	0.344
+34.45 m	3.234/9.5	1.301/2.2	0.768	0.364
+42.65 m	5.108/9.5	1.297/2.2	1.109	0.386

and 3D isolated NI building were conducted, and the isolation effectiveness of 3D-CIB with different vertical stiffness was analyzed. The main conclusions can be drawn as follows.

(1) Both the horizontal and vertical isolation frequencies of 3D isolated NI building were significantly reduced. The horizontal isolation frequency was not only determined by the horizontal stiffness, but also influenced by the vertical stiffness of 3D-CIB, and the vertical isolation frequency decreased with a decrease in the vertical stiffness.
(2) Through the behavior of vertical displacement of 3D-CIB and the horizontal displacement of the superstructure, it can be inferred that the decrease in the vertical stiffness of 3D-CIB may increase the rocking effect. Overall, the rocking effect of this NI building is not obvious.
(3) 3D-CIB can significantly attenuate the horizontal acceleration response of NI building, and a reduction of approximately 80% for the roof was obtained. Also, a fair amount of the vertical acceleration response reduction of the upper structure was still observed. The smaller the vertical stiffness of 3D-CIB is, the better the vertical acceleration isolation effectiveness is.
(4) 3D-CIB can greatly reduce the horizontal FRS, the reduction ratio of the spectral peak values reached 80%. The peak values of vertical FRS decreased and shifted to the lower frequency range, and the spectral values at the right side of spectral peak also decreased with a decrease in the vertical stiffness of 3D-CIB. Additionally, the peak value and ZPA of vertical FRS basically do not vary with the floor height. Thus, it is very beneficial to the vertical seismic design of secondary systems located on high floor.
(5) 3D-CIB exhibited good acceleration isolation effectiveness in both horizontal and vertical directions. Although the advantage of 3D-CIB is that the vertical stiffness can be flexibly adjusted, it should be designed by properly accounting for the balance between the isolation effectiveness and displacement control including rocking effect.

Declaration of competing interest

The authors declare that they have no known competing financial interests or personal relationships that could have appeared to influence the work reported in this paper.

Acknowledgements

This work was supported by the national science and technology major project of advanced technology research on structural health inspection and evaluation of NPPs (Grant No. 2018ZX06002008), and national key project of research on earthquake emergency disposal technology of NPPs (Grant No. 2017YFC1500804). This financial support is gratefully acknowledged.

References

[1] A.A. Markou, G. Stefanou, G.D. Manolis, Stochastic response of structures with hybrid base isolation systems, Eng. Struct. 172 (2018) 629e643.
[2] D. De Domenico, E. Gandelli, V. Quaglini, Effective base isolation combining low-friction curved surface sliders and hysteretic gap dampers, Soil Dynam. Earthq. Eng. 130 (2020) 105989.
[3] A. De Luca, L.G. Guidi, Base isolation issues in Italy: integrated architectural and structural designs, Soil Dynam. Earthq. Eng. 130 (2020) 105912.
[4] A. De Luca, L.G. Guidi, State of art in the worldwide evolution of base isolation design, Soil Dynam. Earthq. Eng. 125 (2019) 105722.
[5] R. Lo Frano, G. Forasassi, Isolation systems influence in the seismic loading propagation analysis applied to an innovative near term reactor, Nucl. Eng. Des. 240 (2010) 3539e3549.
[6] A.S. Whittaker, M. Kumar, Seismic isolation of nuclear power plants, Nuclear Engineering and Technology 46 (2014) 569e580.
[7] A.S. Whittaker, P. Sollogoub, M.K. Kim, Seismic isolation of nuclear power plants: past, present and future, Nucl. Eng. Des. 338 (2018) 290e299.
[8] Ch Coladant, Seismic isolation of nuclear power plants-EDF's philosophy[J], Nucl. Eng. Des. 127 (1991) 243e251.
[9] R. Lo Frano, Benefits of seismic isolation for nuclear structures subjected to severe earthquake, Science and Technology of Nuclear Installations (2018) 1e11. Article ID 8017394,page.
[10] K.L. Ryan, S. Soroushian, E.M. Maragakis, E. Sato, T. Sasaki, T. Okazaki, Seismic simulation of an integrated ceiling-partition wall-piping system at E-Defense. I: three-dimensional structural response and base isolation, J. Struct. Eng. 142 (2016), 04015130.
[11] A.J. Papazoglou, A.S. Elnashai, Analytical and field evidence of the damaging effect of vertical earthquake ground motion, Earthq. Eng. Struct. Dynam. 25 (1996) 1109e1137.
[12] Y. Bozorgnia, M. Niazi, K.W. Compbell, Characteristics of free-field vertical ground motion during the Northridge Earthquake, Earthq. Spectra 11 (4) (1995) 515e525.
[13] J. Xie, Z. Wen, Characteristics of near-fault vertical and horizontal ground motion from the 2008 Wenchuan earthquake, Chin. J. Geophys. 53 (8) (2010) 1796e1805.
[14] J. Suhara, R. Matsumoto, S. Oguri, Y. Okada, K. Inoue, K. Takahashi, 3-D seismic isolation device with rolling seal type air spring, in: 18th International Conference on Structural Mechanics in Reactor Technology (SMiRT18), SMiRT18, Beijing, China, 2005, pp. 3381e3391.
[15] M. Morishita, K. Inoue, T. Fujita, Development of three-dimensional seismic solation systems for fast reactor application, Journal of Japan Association for Earthquake Engineering 4 (2004) 305e310.
[16] J. Suhara, T. Tamura, Y. Okada, K. Umeki, Development of three dimensional seismic isolation device with laminated rubber bearing and rolling seal type air spring, in: ASME 2002 Pressure Vessels and Piping Conference, vol. 2, American Society of Mechanical Engineer, Vancouver, BC, Canada, 2002, pp. 43e48.
[17] A. Kashiwazaki, T. Shimada, T. Fujiwaka, S. Moro, Study on 3-dimensional base isolation system applying to new type power plant reactor, in: Transaction of the 17th International Conference on Structural Mechanics in Reactor Technology (SMiRT 17), vol. 2, SMiRT17, Prague, Czech Republic, 2003.
[18] S. Kitamura, S. Okamura, K. Takahashi, Experimental study on vertical component seismic isolation system with coned disk spring, in: Proceedings of the ASME Pressure Vessels and Piping Conference-Seismic Engineering, 2005, pp. 175e181. Denver, Colorado, USA.
[19] S. Kitamura, M. Morishita, Study on vertical component seismic isolation system with coned disk spring, in: Pressure Vessels and Piping Division, San Diego, California, USA, 2004, pp. 21e28.
[20] M. Morishita, S. Kitamura, S. Moro, Y. Kamishima, S. Takahiro, Study on 3-dimensional seismic isolation system for next generation nuclear power plant-vertical component isolation system with coned disk spring, Technical Report No. 620, in: Proceedings, 13th World Conference on Earthquake Engineering, 2004. Vancouver, BC, Canada.
[21] S. Okamura, Y. Kamishima, K. Negishi, Y. Sakamoto, S. Kitamura, S. Kotake, Seismic isolation design for JSFR, J. Nucl. Sci. Technol. 48 (2011) 688e692.
[22] A. Matsuda, S. Yabana, Evaluation for mechanical properties of laminated rubber bearings using finite element analysis, J. Pressure Vessel Technol. 126 (1) (2004) 134e140.
[23] F. Naeim, J.M. Kelly, Design of Seismic Isolated Structures: from Theory to Practice, John Wiley & Sons Inc, 1999.
[24] W. Witarto, S.J. Wang, C.Y. Yang, J. Wang, Y.L. Mo, K.C. Chang, Yu Tang, Three-dimensional periodic materials as seismic base isolator for nuclear infrastructure, AIP Adv. 9 (4) (2019), 045014.
[25] Y.L. Mo, W. Witarto, K.-C. Chang, S.-J. Wang, Y. Tang, R.P. Kassawara, Periodic material-based three-dimensional (3D) seismic base isolators for small modular reactors, in: Concrete Structure in Earthquake, 2019, pp. 1e16. Singapore.
[26] Z. Zhou, J. Wong, S. Mahin, Potentiality of using vertical and three-dimensional isolation systems in nuclear structures, Nuclear Engineering and Technology 48 (5) (2016) 1237e1251.
[27] J.O. Almen, A. Laszlo, The Uniform-Section Disc Spring vol. 58, Transactions of American Society of Mechanical Engineers, 1936, pp. 305e314. RP-58-10.
[28] China National Standardization Management Committee, Disc spring (2005) (GB/T1972-2005).
[29] Y. Zhao, J. Su, X. Zhou, Y. Sui, Design and performance test of combined disk spring bearing for vertical-isolated buildings, J. Beijing Univ. Technol. 35 (7) (2009) 892e898.
[30] Westinghouse Electric Corporation, AP1000 design control document, Rev. 19 (2011).
[31] RG 1.60, Rev.1, Design Response Spectra for Seismic Design of Nuclear Power Plants, U.S. Nuclear Regulatory Commission, 1973.
[32] RG 1.92, Rev.2, Combining Modal Responses and Spatial Components in Seismic Response Analysis, U.S. Nuclear Regulatory Commission, 2006.